15TH IEA HEAT PUMP CONFERENCE
MAY 26–29, 2026 | HOFBURG
VIENNA 2026
DECARBONISATION THROUGH INNOVATION

Parametric energy analysis of alternative layouts for an R718 high-temperature heat pump - insights from the GEOSYN project

A. Zini[a*], O.M. Moen[b], K. Banasiak[b], J. R. Dowdell[b], S. Sannan[b], P. Gullo[c], V. Somasundaram[c], M. Dallai[d], G. Vitri[e], F. Luchetti[e], A. Rocchetti[a], A. Milazzo[a], and L. Talluri[a]

a Thermodynamics and Heat Transfer Research Group – Department of Industrial Engineering, University of Florence (Italy)
b SINTEF Energy Research, Sem Sælands vei 11, Trondheim, 7034, Norway
c University of Southern Denmark (SDU), Institute of Mechanical and Electrical Engineering, Alsion 2, Sønderborg, 6400, Denmark
d Officine Mario Dorin S.p.A., Florence, 50061, Italy
e Rivacold srl, Vallefoglia, Pesaro Urbino (Italy)

Abstract

The recovery of medium- to high-temperature waste heat remains a significant challenge in industrial applications, particularly for high-temperature heat pumps, which often struggle to source heat at the required temperatures for effective operation. The GEOSYN Horizon Europe project addresses this issue by developing an innovative R718 high-temperature heat pump that harnesses medium-enthalpy geothermal energy, delivering 50 kW of process heat at 200 ºC to a local dairy plant and achieving a temperature lift of at least 80 K. Water offers several advantages as a high-temperature working fluid, including low cost, wide availability, zero environmental impact, non-toxicity, and non-flammability. However, it also presents significant challenges, such as high specific volume, large compression ratios, and high discharge temperatures, which must be addressed to fully exploit its potential. A preliminary energy analysis was conducted to assess how different system configurations respond to variations in key thermodynamic and technical parameters, including evaporation and condensation temperature levels, suction superheat, and the number of compression stages. Parametric analyses were performed to evaluate the effects on overall performance, compression ratios, volumetric heating capacity, and discharge temperatures. Open intercoolers yielded the highest COP of 3.87 under design conditions, though at the cost of increased system complexity. In contrast, closed intercoolers resulted in slightly lower performance but provided a more practical solution, effectively addressing the main technical challenges. These analyses provided a basis for component selection, particularly for the compressor, and for the initial performance evaluation, thereby guiding the design of the complete machine optimized for high-temperature industrial heat recovery.

Keywords: High temperature heat pump; R718; steam compressor; industrial process steam production; renewable energy

1. Introduction

1.1. The industrial context

High-temperature industrial heat pumps represent a pivotal emerging key technology for improving energy efficiency and reducing the environmental impact of industrial thermal processes, showing significant potential

* Corresponding author. Tel.: +39 3804337930
E-mail address: andrea.zini@unifi.it

as alternatives to fossil-fuelled boilers in sectors such as pulp and paper, food and beverage, chemicals, pharmaceuticals, non-metallic minerals, and machinery, which require heat above 200 ºC.

Achieving such high temperature levels requires suitable components and carefully selected working fluids. Increasingly strict environmental regulations on conventional refrigerants make the identification of new, sustainable fluids essential. These working fluids must ensure good thermodynamic performance while presenting zero ODP, negligible GWP, no PFAS content, and minimal risks for human health.

The deployment of this technology aligns with international decarbonization strategies, including initiatives such as the European Green Deal, which targets climate neutrality in the EU by 2050. In this context, high-temperature industrial heat pumps represent a crucial technology for enabling cleaner and more efficient industrial energy systems. Nonetheless, technological challenges remain, particularly regarding efficiency, reliability, and cost-effectiveness of these systems.

1.2. The GEOSYN Project

The GEOSYN project ("GEOthermal SYNergy: Enhancing Industrial Energy Efficiency Through Steam High-Temperature Heat Pumps and Heat-Powered Cooling Systems with Operational Flexibility and Public Trust"), funded under the Horizon Europe programme, aims to address these challenges by developing an integrated solution that harnesses geothermal waste heat. The system will deliver 50 kW of process steam at 200 ºC to a dairy industry (cheese production) using an R718 high-temperature heat pump. In parallel, it will provide 20 kW of refrigeration capacity via a heat-powered cooling system to cool a refrigerated warehouse down to 12 ºC (Figure 1).

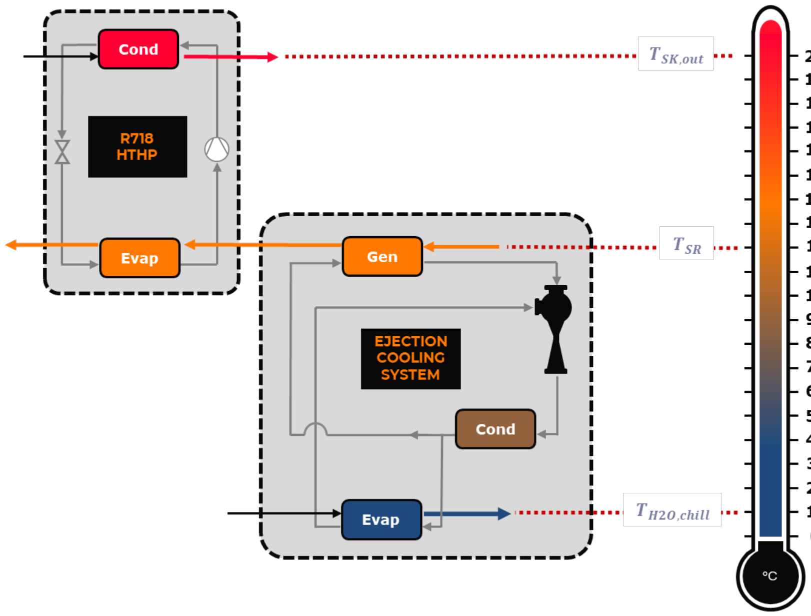

Figure 1: GEOSYN project concept design

1.3. Objectives of this work

This work forms part of the GEOSYN project and contributes to the exploratory assessment of current technological options for generating process steam using heat pump systems. A preliminary selection of state-of-the-art working fluids for high-temperature industrial heat pumps has been carried out and compared with the potential use of water as an alternative working fluid. The availability of medium- to high-temperature waste-heat sources (>80–100 ºC) helps to overcome several technical challenges typically associated with operating water at very low evaporation pressures. Furthermore, the analysis considers the use of additional components intended to enhance the performance of water-based cycles within the temperature range relevant to the GEOSYN project.

2. Materials and methods

2.1. Working fluids preliminary selection – benefits and issues of using R718

The selection of the working fluid is a crucial aspect in the design of a heat pump, with its choice being subject to several factors. The thermodynamic performance is not the only requirement to be considered; working fluids must also be evaluated in relation to safety and environmental prescriptions given by several legislative limitations. The comparative findings reported in [1] offered useful guidance for the broader assessment of candidate working fluids, highlighting those with potential within the temperature ranges relevant to industrial applications. Out of the 25 pure fluids initially examined, three were selected for further investigation in this study and comparison with R718, as summarised in Table 1.

Table 1:Properties of the working fluids selected for the analysis

Fluid	**T_{crit}** [°C]	**P_{crit}** [bar]	**NBP** [°C]	**T_{auto}** [°C]	**SC**
R1233zd(E)	165.6	35.73	18.26	-	A1
R601	196.5	33.64	35.87	258	A3
Cyclopentane	238.6	45.71	49.26	361	A3
Water	373.9	220.64	99.97	-	A1

Several considerations motivated the selection of these fluids. Although all candidates examined comply with current F-Gas regulations regarding GWP and ODP limits, an additional concern arises from the formation of PFAS degradation products, a topic not yet comprehensively regulated [2,3]. Among the available options, R1233zd(E) was identified as a particularly promising candidate for high-temperature heat pump applications. Its selection is primarily justified by its significantly lower molar yield of TFA upon degradation (approximately 2%) compared with the near-complete conversion observed for R1224yd(Z) and the roughly 20% yield reported for R1336mzz(Z) [4,5], as well as by its superior thermodynamic performance within the temperature range of interest [1]. Among the fluids listed in Table 1, R1233zd(E) represents the option with the highest current Technology Readiness Level (TRL 9) and is safe from both a toxicity and flammability standpoint.

The use of hydrocarbons (HC) in refrigeration and heat pump technologies is now well established. R601 (n-Pentane) was selected as the representative alkane (HC) in this study, as it exhibits a TRL comparable to that of synthetic fluids. In addition, it offers superior performance relative to its isomers (isopentane and neopentane). Alkanes with more than five carbon atoms, although potentially promising from a performance standpoint, have not yet reached an adequate level of technological maturity and present increasingly critical issues related to flammability and auto-ignition risk. Cyclopentane was included because it represents one of the non-standard working fluids currently progressing in TRL for high-temperature heat pump applications. Moreover, it is the only viable alternative (non-toxic and technically feasible) to water for producing process steam above 10 bara.

R718 is the most economical and widely distributed natural refrigerant worldwide, being non-toxic and non-flammable. Its thermodynamic properties offer high potential for HTHP applications, especially for extreme thermal levels. However, significant challenges persist in its use in vapour compression cycles: many prototypes of R718 cycles have been realised, including at high TRLs, but their commercial diffusion is still limited [6,7]. Water's high polytropic exponent, high specific volume of steam, and low molecular weight result in excessively high discharge temperatures, volumetric flow rates, and compression ratios. Its normal boiling point (NBP) is 100 ºC, necessitating evaporation at pressures lower than atmospheric (sometimes significantly lower).

2.2. Numerical thermodynamic models

Considering the temperature lifts involved, three different cycle layouts were analysed depending on the working fluid:

- Standard layout without intercooling (STD): Suitable for synthetic working fluids (R1233zd(E), and HCs (Pentane, Cyclopentane), owing to their characteristic upper-limit curves, which ensure that compressor discharge temperatures remain within acceptable bounds, thus eliminating the need for intercooling during the compression process (Figure 2a).
- Multistage layout with intercooling (MS-IC): Applicable for R718, which exhibits a negative inclined upper-limit curve, leading to technically unsustainable discharge temperatures and extremely high compression ratios unless multistage compression with intercooling is adopted (Figure 2b).
- Cascade layout (CAS): In this configuration, the single heat pump used in the previous layouts is divided into two units, denoted the "bottomer" and the "topper," connected by an intermediate heat exchanger acting as the condenser for the bottomer and the evaporator for the topper (Figure 2c).

The following assumptions were made for the simulation: steady-state operation, no heat exchange with surroundings, and no pressure losses in heat exchangers or piping. The imposed heat-exchanger conditions are shown in Table 2.

Table 2: Imposed conditions inside the heat exchangers

Physical quantity	Abbreviation	Value
Source temperature difference	ΔT_{SR}	10 K
Temperature difference between sink outlet and condensation level	ΔT_{cond}	5 K
Temperature difference between source outlet and evaporation level	ΔT_{evap}	5 K
Useful superheating inside the evaporator	$\Delta T_{SH,u}$	5K
Useful subcooling inside the condenser	$\Delta T_{SC,u}$	0 K
Temperature difference inside cascade heat exchanger	ΔT_{CAS}	7 K
Temperature difference above saturation point at the outlet of ICs	ΔT_{IC}	20 K

Evaporation and condensation temperature were calculated using:

$$T_{evap} = T_{SR,out} - \Delta T_{evap} \tag{1}$$

$$T_{cond} = T_{SK,vap} + \Delta T_{cond} \tag{2}$$

An internal regenerative heat exchanger (IHX) was included in all configurations to provide additional superheating beyond that achievable in the evaporator, adjusted via the thermostatic expansion valve. Additional superheating benefits all tested fluids. For fluids with positively sloped upper-limit curves it improves performance [1,8] and is technically necessary to avoid wet compression. For fluids with bell-shaped curves (R718), it does not significantly affect performance but is crucial when employing oil-free, self-lubricated compressors to prevent suction near the two-phase region. The IHX was modeled assuming a heat-exchanger effectiveness of 0.3 according to Kays & London:

$$\varepsilon_{IHX} = \frac{\dot{Q}}{\dot{Q}_{max}} = \frac{\dot{Q}}{(\dot{m}\cdot cp)_{min}\cdot \Delta T_{max}} \tag{3}$$

The multistage design was automated to allow variation in the number of stages based on the overall compression ratio. A maximum compression ratio per single stage of 2.5 was assumed. The overall compression ratio was distributed geometrically according to Equation (4), and the number of stages was rounded up to the next integer (Equation (5)). The effective per-stage compression ratio was then recalculated in Equation (6). Compression was modelled assuming a constant isentropic efficiency of 0.75.

$$\beta_{stage,max} = \beta^{1/NS} \tag{4}$$

$$NS_{new} = ceil(NS) \tag{5}$$

$$\beta_{stage,new} = \beta^{1/NS_{new}} \tag{6}$$

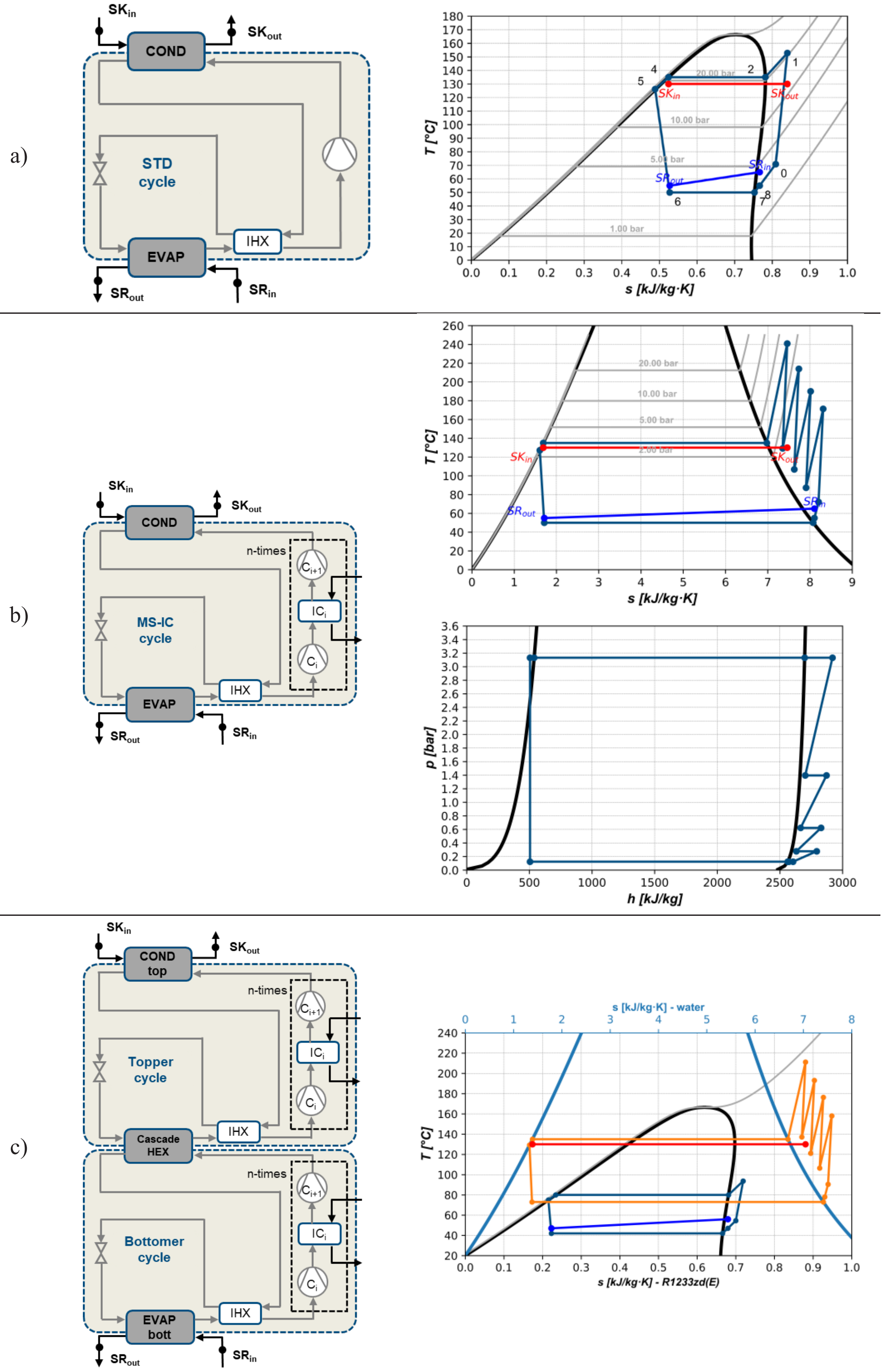

Figure 2: a) Standard layout (STD) with related T-s diagram (R1233zd(E) as example); b) Multistage intercooled layout (MS-IC) with related T-s and p-h diagrams (R178 as example); c) Cascade layout (CAS) with T-s diagram (R1233zd(E) as bottomer cycle working fluid and R718 as topper working fluid as example);

For the MS-IC layout, the working fluid was cooled between the discharge of one stage and the suction of the next using an intercooler, providing at least 20 K of superheating at the outlet (analogous to the IHX reasoning for R718).

For the CAS layout, the bottomer condensation temperature was fixed, and the topper evaporation temperature was calculated assuming a 7 K temperature difference. The mass flow rate of the topper cycle was set to match the bottomer condenser capacity.

Performance was calculated as the ratio of useful power to the total compressor input power. In the CAS layout, the total compressor input power included the sum of the compressor powers of both the bottomer and topper cycles.

The first comparison analysis was conducted using fixed boundary conditions for the evaporator, specifying the inlet and outlet temperature and pressure of the cold source, together with a source mass flow rate of 1 kg/s. This allowed the results to be presented in a dimensionless, scalable form. The hot-sink temperature was varied between 120 ºC and 200 ºC, assuming complete vaporization (from saturated liquid, x = 0, to dry saturated vapour, x = 1). The coefficient of performance, the processable hot-sink flow rate, and the working fluid mass flow rate were calculated and compared.

The use of R718 was compared with Cyclopentane under the boundary conditions of the GEOSYN project. In particular, the evaporation temperature was fixed at 100 ºC and the condensation temperature at 205 ºC, with the objective of producing 50 kW of dry saturated steam at 200 ºC (15.55 bara). All previously stated assumptions and hypotheses concerning the heat exchangers in Table 2 were considered valid.

The feasibility of using R718 with interstage cooling not only through a closed heat exchanger (intercooler), but also by liquid injection into the manifold between the discharge of one stage and the suction of the next (open or mixing-type intercooler), was also evaluated. The potential use of a flash tank as a performance-enhancing component was assessed in combination with both interstage cooling strategies. Figure 3 shows the corresponding layouts and T–s diagrams, where the subscript i ranges from 1 to $N_S - 1$.

Cooling by liquid injection (LI layout in Figure 3a) allows the steam between two compression stages to be cooled by absorbing heat and thereby completely vaporizing the injected flow $F_{\mathrm{inj},i}$. In practice, this injected stream is not pure liquid ($x = 0$) but a two-phase mixture with a relatively low quality, still providing a substantial amount of latent heat. The required injection fraction is determined from the enthalpy balance and the continuity equation:

$$m\left[F_{inj,i}\right] \cdot \Delta h_{F_{inj,i}} = m\left[C_{suct,i+1}\right] \cdot h_{C_{suct,i+1}} - m\left[C_{disch,i}\right] \cdot h_{C_{disch,i}} \tag{7}$$

$$m\left[F_{inj,i}\right] + m\left[C_{disch,i}\right] = m\left[C_{suct,i+1}\right] \tag{8}$$

The liquid separator, or flash tank, is widely employed in refrigeration. After an initial throttling step, part of the flow flashes to the discharge pressure of the i-th stage, producing a two-phase stream that separates into a saturated liquid fraction ($x = 0$) at the bottom of the tank and dry saturated vapour ($x = 1$) at the top. The vapour fraction depends on the quality of the two-phase flow and is calculated as:

$$m\left[FT_{vap,i}\right] = m\left[DF_i\right] \cdot x_{DF_i} \tag{9}$$

The injection of dry saturated vapour at the compressor suction naturally reduces the temperature of the superheated vapour exiting the i-th intercooler. A conservative superheating margin of 20 K was imposed downstream of this mixing process (FT-IC layout, Figure 3b). The saturated liquid fraction is then further expanded, and the procedure is repeated for each compression stage.

The flash tank was also evaluated in combination with liquid-injection cooling. In this configuration, the injected fraction is saturated liquid ($x = 0$), rather than a two-phase mixture as in the LI layout, providing the full amount of latent heat available at the flash-tank pressure for cooling in the manifold. In this case, the energy balance includes both liquid injection and the injection of flash vapour at the compressor suction, combining Equations (7) and (8) with Equation (9).

All models were implemented in Python, using NIST REFPROP v10 [9] for fluid property calculations.

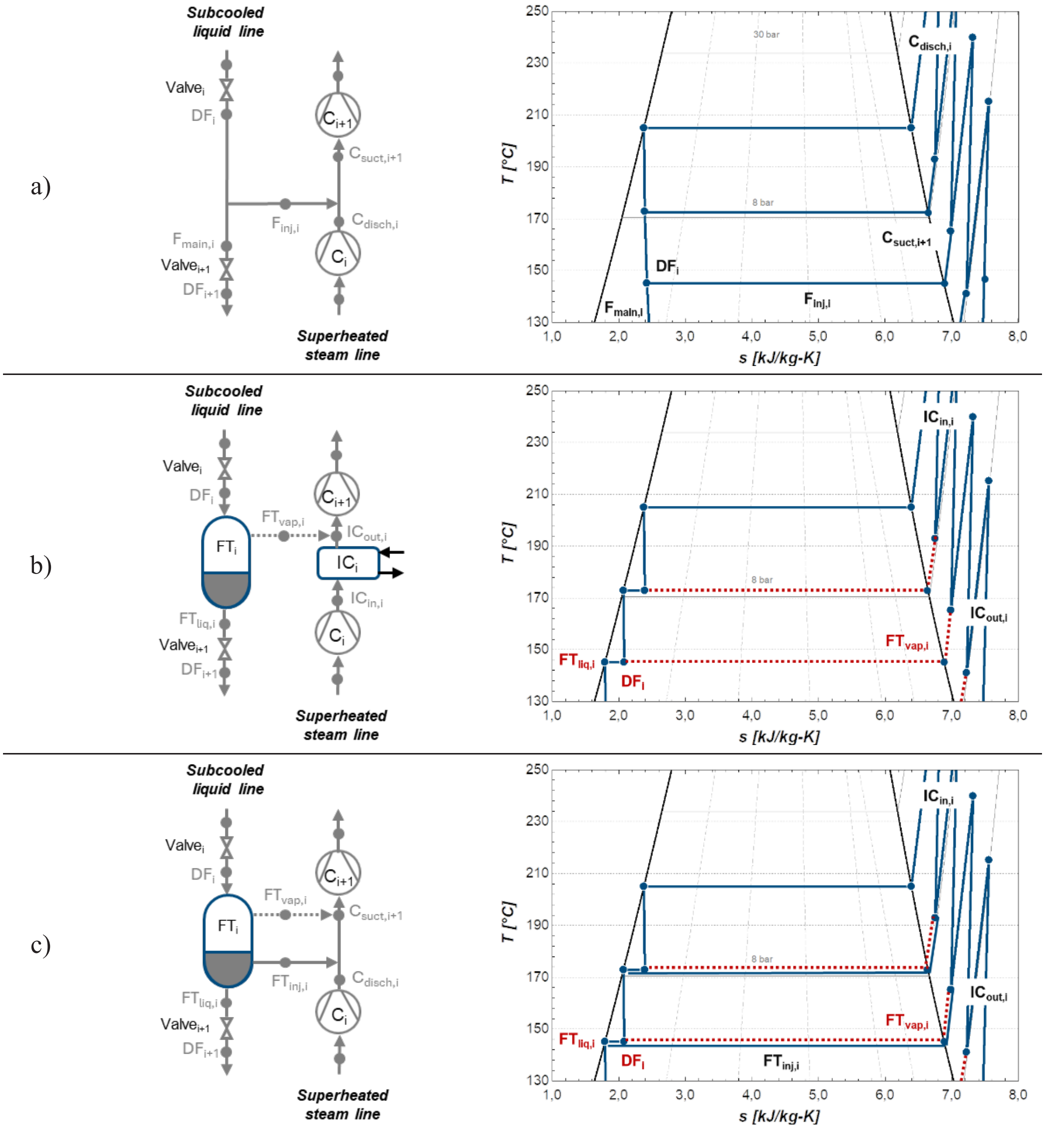

Figure 3: Layout and T-s diagram for a) R718 Liquid injection (STD); b) R718 flash tank and intercooler (FT+IC); c) R718 flash tank and liquid injection (FT+LI).

3. Results

3.1. Comparison of R718 HTHP with other working fluids

Figure 4 presents a comparison of the coefficient of performance, the processable sink mass flow rate $\dot{m}_{SK}$, and the topper working fluid mass flow rate $\dot{m}_{ref,top}$ for the CAS layout: R718 was used as the topper fluid, while the three previously described working fluids (R1233zd(E), R601, and Cyclopentane) served as bottomers.

As expected, the COP decreases with increasing temperature lift. The processable hot-sink mass flow rate, on the other hand, increases because higher compression work raises the power available at the condenser, while the latent heat of vaporization of the hot sink decreases. The topper working fluid mass flow rate also increases with rising temperature lift due to higher throttling losses: to vaporize the hot sink at higher temperatures (i.e., to provide saturated vapour at higher pressures), the inlet quality at the evaporator decreases, requiring a higher bottomer-fluid mass flow rate to extract the same amount of power from the cold source.

Overall, the trends are consistent and nearly overlapping. The maximum deviation in performance is +2.8% at T_{SK_vap} = 120 ºC for Cyclopentane + R718 relative to R1233zd(E) + R718, decreasing to +1.2% at

$T_{SK\_vap} = 200$ ºC .Similarly, the processable hot-sink mass flow rate is almost insensitive to the choice of bottomer fluid, with a constant difference of +1.1% for R1233zd(E) + R718 relative to Cyclopentane + R718 across the entire vaporization temperature range.

The change in the slope of the curve for the processable hot-sink mass flow rate is due to the fact that, as the temperature lift increases, the thermodynamic model automatically adjusts the number of compression stages of the topper cycle to maximize the COP for the given configuration.

Given the very small variation in trends across different bottomer fluids, the subsequent comparisons with alternative layouts focus solely on the R1233zd(E) + R718 combination. This choice ensures both full technological maturity and maximum safety (A1 classification).

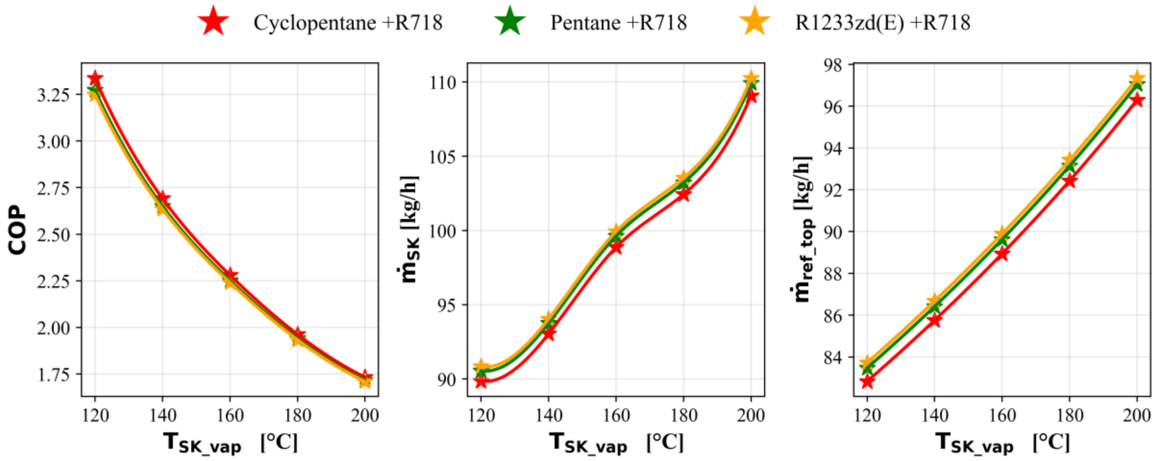

Figure 4: Trends of performance (COP), mass flow rate of the hot sink produced ($\dot{m}_{SK}$), and mass flow rate of the working fluid in the topper cycle($\dot{m}_{ref,top}$), respectively from left to right, as a function of the produced steam temperature for the three CAS-layout combinations.

The results shown in Figure 4 were obtained by fixing the condensation temperature of the bottomer at 90 ºC. Further optimization of this condensation level would be desirable in principle. However, this assumption was chosen because such optimization is highly dependent on the specific boundary conditions. Moreover, setting the same temperature for all three fluids ensures that the results remain general and comparable. The value of 90 ºC was selected to ensure that the topper cycle operates close to the GEOSYN boundary conditions while also guaranteeing a high overall TRL. Indeed, steam compressors operating under partial-vacuum conditions at these temperatures are widely used in mechanical vapour recompression applications and are technically mature and commercially available.

Figure 5 presents the same comparison metrics for all configurations and working fluids listed in the legend. The observed trends and underlying mechanisms are similar to those discussed for Figure 4.

R1233zd(E) and R601 are naturally limited to generating saturated vapour only up to certain temperatures. Both represent the state of the art (highest TRL) for closed-cycle vapour generation via vapour-compression heat pumps. R718 exhibits slightly lower COP values compared to Cyclopentane at low hot-sink temperatures, with the trend reversing as the pressure of the generated vapour increases.

The processable hot sink mass flow rate is strongly influenced by the working fluid. Due to its high latent heat, R718 requires a significantly lower mass flow rate than the other refrigerants to extract the same power from the cold source. Consequently, the available power at the condenser is lower, which, combined with the relatively low compression work under multistage intercooling, results in a limited processable hot-sink mass flow rate.

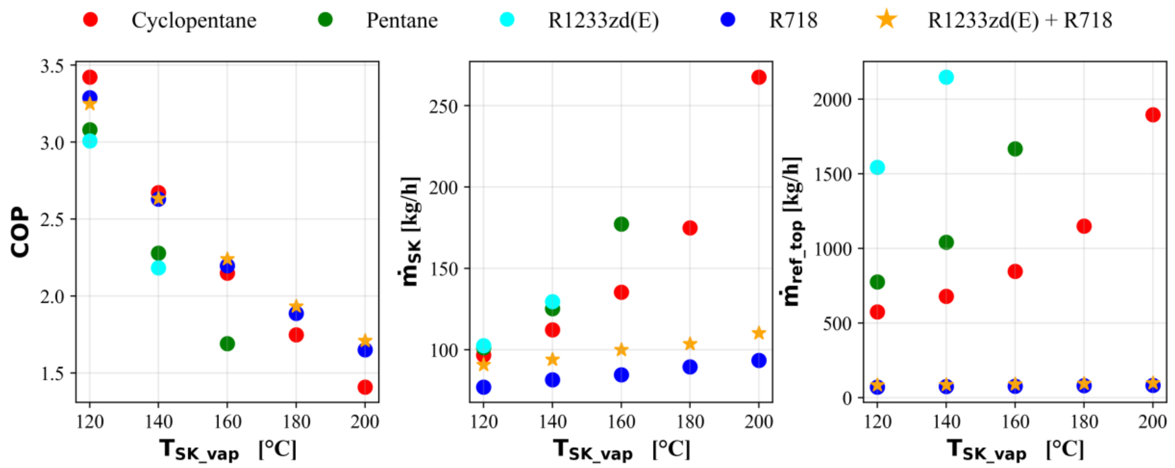

Figure 5: Trends of performance (COP), mass flow rate of the hot sink produced ($\dot{m}_{SK}$), mass flow rate of the working fluid ($\dot{m}_{ref}$), respectively from left to right, as a function of the produced steam temperature for different working fluids

Figure 6 shows the percentage increases relative to the values reported in Figure 5, calculated using the lowest value for each configuration as the reference (indicated below each hot-source temperature on the x-axis).

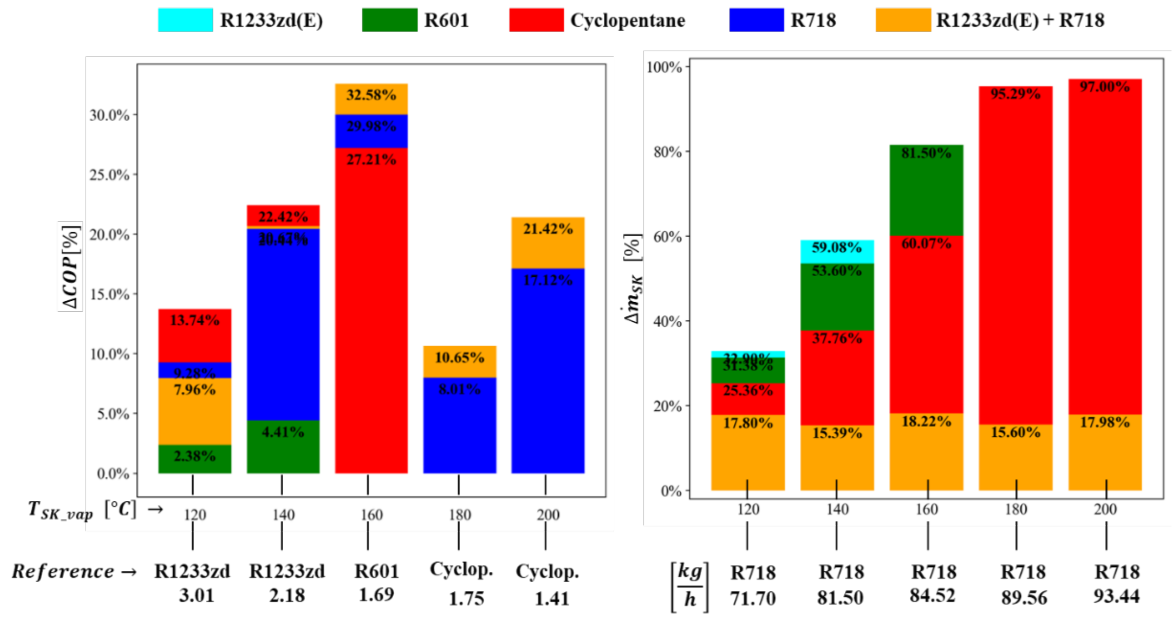

Figure 6: Percentage increase of performance (ΔCOP, left) and hot-sink mass flow rate ($\Delta\dot{m}_{SK}$, right) with respect to the reference value (shown on the x-axis) as a function of the produced steam temperature for different working fluids.

3.2. Comparison of performance enhancing layouts for R718 HTHP

Figure 7 shows the comparison between Cyclopentane (STD layout with the assumptions from the first part of Section 2.2) and R718 (in the layouts and with the assumptions explained in the second part of Section 2.2) under boundary conditions similar to those imposed by the GEOSYN project: evaporation fixed at 100 ºC and production of 50 kW of dry saturated steam at 200 ºC (starting from saturated liquid at the same pressure, 15.55 bara).

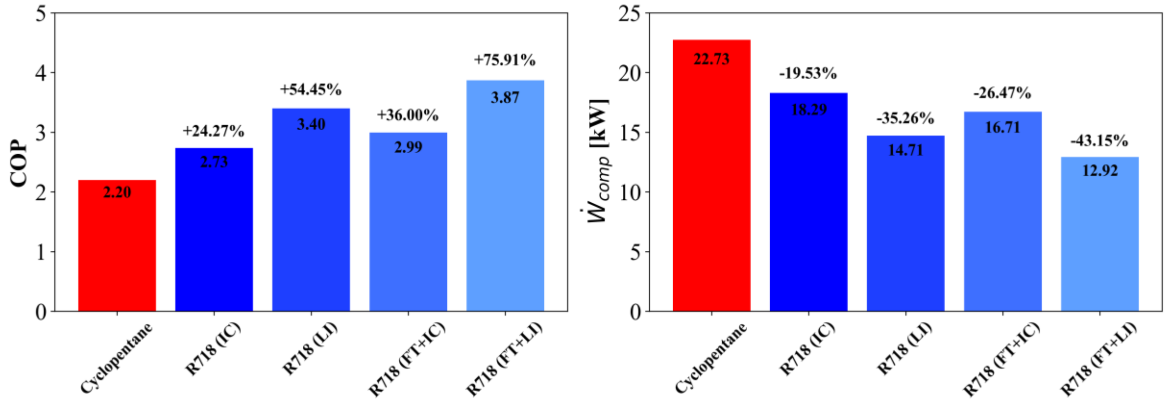

Figure 7: Comparison of Cyclopentane and R718 (with different layouts) in terms of performance and compressor power consumption for a produced steam temperature of 200 ºC and an evaporation temperature of 100 ºC.

When evaporation temperatures reach high values, namely when waste heat (cold source) temperatures exceed 100 ºC, the use of R718 as the working fluid, even without performance-enhancing components, results in significantly higher performance than Cyclopentane.

The use of liquid injection as the interstage-cooling method further increases the performance gap: the 19.7% improvement compared with using an intercooler can be attributed to the fact that, in the LI layout, the mass flow rate in the lower compression stages decreases due to the three bleed streams required to inject the specified flow rate into the manifold between compression stages, leading to a reduction in the total power consumption (Figure 8). It should also be emphasized that, in configurations employing intercoolers as the interstage-cooling method, the power dissipated in the closed heat exchangers was assumed to be released to the environment and therefore not counted as useful effect in the performance calculation.

The same effect of reduced mass flow rate in the lower compression stages also occurs when using flash tanks: their inclusion increases performance by 8.7% and 12.14%, respectively, compared with the IC and LI configurations. The reason for the larger increase in the FT+LI case is that this configuration introduces two bleed streams for each interstage flash tank, further reducing the flow compared with the FT+IC layout (only one bleed stream per flash tank), as illustrated in Figure 3. The use of flash tanks has an additional beneficial effect: recovery of throttling losses. Because a portion of the flow is flashed before entering the evaporator, the inlet vapour quality decreases, increasing the specific evaporator heat uptake [kJ/kg]. As a result, for the same flow rate, more heat can be extracted from the same waste heat source.

Table 3 lists the absorbed power, injected liquid fractions for cooling ($m\left[F_{\mathrm{inj},i}\right]$or $m\left[FT_{\mathrm{inj},i}\right]$), and injected vapour fractions ($m\left[FT_{\mathrm{vap},i}\right]$) for each stage across the four R718 layouts.

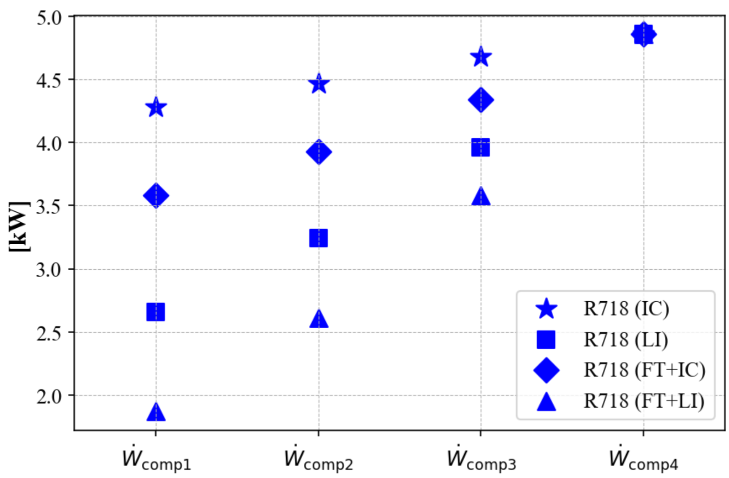

Figure 8: Trends of absorbed power for the four different compression stages for the four different R718 layouts.

Table 3: Values of absorbed power for each compression stage, injected vapour fraction, injected liquid fraction for each intercooling/flash section and quality at the inlet of the evaporator for the four different R718 layouts

Layout	$\dot{W}_{C1}$ [kW]	$\dot{W}_{C2}$ [kW]	$\dot{W}_{C3}$ [kW]	$\dot{W}_{C4}$ [kW]
IC	4.28	4.47	4.68	4.86
LI	2.66	3.24	3.96	4.86
FT+IC	3.58	3.93	4.34	4.86
FT+LI	1.87	2.61	3.58	4.86

Layout	$m[FT_{vap,1}]$	$m[FT_{vap,2}]$	$m[FT_{vap,3}]$	$m[F_{inj,1}]$	$m[F_{inj,2}]$	$m[F_{inj,3}]$	$x_{evap,in}$
IC	-	-	-	-	-	-	0.1919
LI	-	-	-	0.1021	0.1240	0.1526	0.1919
FT+IC	0.0411	0.0525	0.0702	-	-	-	0.0397
FT+LI	0.0273	0.0433	0.0702	0.1194	0.1400	0.1633	0.0397

4. Conclusions

The analysis carried out within the GEOSYN project confirms the potential of high-temperature industrial heat pumps as a key technology to improve energy efficiency and reduce the environmental impact of industrial thermal processes. Among the working fluids considered, water (R718) emerges as a natural and safe alternative with high potential for extreme temperature applications, although technical challenges remain due to its very high compression ratios and elevated discharge temperatures.

Closed-cycle heat pumps were selected for comparison, excluding mechanical vapour recompression systems. This choice reflects the requirements in sectors such as pharmaceuticals and food & beverage, where ultra-pure steam is needed and could be compromised by direct steam compression. Furthermore, in chemical processes, many water-based mixtures (containing diluted chemicals) must remain separated from the production system due to toxicity concerns.

An initial exploratory analysis compared different working fluids and layouts for producing dry saturated steam at temperatures between 120 ºC and 200 ºC (saturation pressures from 2 to 15.55 bara), assuming an evaporation temperature of 50 ºC to simulate a medium-low temperature waste heat source.

High-TRL solutions are limited to steam production up to approximately 160 ºC (around 6 bara). R1233zd(E) shows the lowest performance but offers maximum safety (A1 classification), while R601 achieves higher COPs but presents flammability concerns. Process steam at higher temperatures can be produced using cascade heat pumps. Use of R718 as the topper fluid was explored and found to be largely insensitive to the choice of bottomer fluid. The combination of R1233zd(E) + R718 achieves the target performance with very high TRL. A single water-based heat pump can provide comparable COP but requires sub-atmospheric evaporation when the waste heat source is medium-low temperature. Cyclopentane offers the highest performance but has safety limitations and relatively low TRL.

In a second comparison, the evaporation temperature was increased. For producing dry saturated steam at 200 ºC with 100 ºC evaporation, the only viable options were Cyclopentane or R718. R718 achieves a 24% higher COP than Cyclopentane while maintaining favourably safety characteristics regarding flammability. Both solutions have a TRL not exceeding 6. Interstage cooling via liquid injection outperformed closed intercoolers, increasing COP from 2.73 to 3.40. It should be noted that the modelled steam production, from saturated liquid to dry saturated vapour, does not directly exploit the heat dissipated in intercoolers. If other industrial processes could utilize this heat, the system's overall COP would further increase.

The use of flash tanks, though adding complexity, significantly improves performance (+8.7 % to +12.4 %) by recovering throttling losses and reducing mass flow rates in the lower compression stages, thereby lowering the compressor power demand.

Overall, the results show that R718-based HTHP systems, combined with cycle optimization strategies and advanced components, offer a competitive balance of energy efficiency, safety, and technological feasibility. These systems represent a promising solution for sustainable high-temperature industrial steam production and support the energy transition in industry in line with European decarbonization strategies.

Nomenclature

cond	Condensation / condenser	NS	Number of compression stages
evap	Evaporation /evaporator	SR	Source
HTHP	High temperature heat pump	SK	Sink
IHX	Internal heat exchanger	WHR	Waste heat recovery
m	Mass flow rate fraction (dimensionless)	$\dot{W}$	Compressor work rate
$\dot{m}$	Mass flow rate	$\dot{Q}$	Heat rate exchanged

Acknowledgements

Funding from the Horizon Europe Project GEOSYN - GEOthermal SYNergy: Enhancing Industrial Energy Efficiency Through Steam High-Temperature Heat Pumps and Heat-Powered Cooling Systems with Operational Flexibility and Public Trust (Horizon Europe Programme– Call CL5-2024-D3-01 - G.A. No. 101172812).

References

[1] Zini A, Socci L., Vaccaro G., Rocchetti A., Talluri L. 2024. Working Fluid Selection for High-Temperature Heat Pumps: A Comprehensive Evaluation, Energies 17 (7): 1556, 2024

[2] Glüge, J, Breuer K., Hafner A., Vering C., Müller D., Cousins I.T., Lohmann R., Goldenman G., Scheringer M., Finding Non-Fluorinated Alternatives to Fluorinated Gases Used as Refrigerants. Environmental Science: Processes & Impacts 26 (11): 1955–74, 2024.

[3] Pérez-Peña, M.P., Fisher J.A., Hansen C., Kable S.H., Assessing the Atmospheric Fate of Trifluoroacetaldehyde (CF3 CHO) and Its Potential as a New Source of Fluoroform (HFC-23) Using the AtChem2 Box Model». Environmental Science: Atmospheres 3 (12): 1767–77, 2023

[4] Arpagaus, C and Bertsch S.S., Experimental Results of HFO/HCFO Refrigerants in a Laboratory Scale HTHP with up to 150 °C Supply Temperature, 2nd Conference on High Temperature Heat Pumps, 9th September 2019, Copenhagen, Denmark, 2019

[5] Arpagaus, C., Bless F., Uhlmann M., Schiffmann J., Bertsch S.S., High Temperature Heat Pumps: Market Overview, State of the Art, Research Status, Refrigerants, and Application Potentials. Energy 152, 985–1010, 2018

[6] Hu B., Wu D., Wang R.Z., Water vapor compression and its various applications, Renewable and Sustainable Energy Reviews, Volume 98, 2018, Pages 92-107.

[7] Lazzarin R., Mechanical Vapour Recompression (MVR): a review of applications and a comparison with Thermal Vapour Recompression (TVR), ICR2023 | 26thInternational Congress of Refrigeration | August 21st-25th, 2023 | Paris, France

[8] Arpagaus C., Bless F., Uhlmann M., Schiffmann J, Bertsch S.S., High temperature heat pumps: Market overview, state of the art, research status, refrigerants, and application potentials, Energy, 2018

[9] Lemmon E.W., Huber M.L., McLinden M.O., NIST Standard Reference Database 23: Reference Fluid Thermodynamic and Transport Properties-REFPROP, Version 10